Synchrotron-radiation X-ray topography of surface strain in large-diameter silicon wafers

S. Kawado,[a]* S. Iida,[b] S. Yamaguchi,[b] S. Kimura,[c] Y. Hirose,[d] K. Kajiwara,[e] Y. Chikaura[f] and M. Umeno[g]

[a]Rigaku Corporation, Akishima-shi, Tokyo 196-8666, Japan, [b]Department of Physics, Toyama University, Toyama 930-8555, Japan, [c]System Devices and Fundamental Research, NEC Corporation, Tsukuba 305-8501, Japan, [d]TOYOTA Central R&D Laboratories Inc., Nagakute-cho, Aichi 480-1192, Japan, [e]Japan Synchrotron Radiation Research Institute, SPring-8, Mikazuki-cho, Hyogo 679-5198, Japan, [f]Faculty of Engineering, Kyushu Institute of Technology, Kitakyushu-shi 804-8550, Japan, and [g]Graduate School of Engineering, Osaka University, Suita, Osaka 565-0871, Japan. E-mail: kawado@rigaku.co.jp

Using a 300 mm-wide monochromatic X-ray beam obtained at beamline BL20B2 of SPring-8, the difference in surface-strain distribution caused by various steps of silicon-wafer manufacturing, *i.e.* slicing, lapping, etching, grinding and polishing, was studied. The asymmetric 511 reflection of 21.45 keV X-rays, incident at a glancing angle of 0.26°, was used to obtain topographs over the whole surface of a 200 mm-diameter (100) CZ silicon wafer. Differences in crystallinity and in warp between the surfaces at different steps of the manufacturing process (firstly after the lapping following the slicing, and then after successive etching, grinding and polishing) were clearly observed. The former gave a topographic image over the whole area with a one-shot exposure because of their wide rocking curves (50–70 arcsec FWHM), which indicate poor crystallinity. The latter, on the other hand, showed sharper curves (4–5 arcsec FWHM), which indicate good crystallinity in local areas, and the existence of warp, and therefore required step scanning of ω-rotation to cover the whole surface in topography measurements. The effect of each step in the process is also discussed.

Keywords: X-ray topography; asymmetric reflection; silicon wafers; surface strain.

1. Introduction

X-ray diffraction topography has been usefully applied to the characterization of microdefects (Chikawa *et al.*, 1970; Ishikawa, 1989; Iida *et al.*, 1990), growth striations (Kawado *et al.*, 1990; Kudo *et al.*, 1997) and process-induced defects (Tanner, 1976; Boller *et al.*, 1998; Kudo *et al.*, 2001) in silicon. The techniques used in these studies were well sophisticated in most cases. They were, however, unsuitable for practical application, *e.g.* inspection of as-received silicon wafers used for the LSI fabrication.

Surface-sensitive topography is very useful because semiconductor devices are formed in the surface layers of wafers. Synchrotron plane-wave X-ray topography of 150 mm-diameter silicon wafers was realised at the Photon Factory and revealed growth striations and surface-strain distribution (Kitano *et al.*, 1987).

Recent industrialization of 200 mm- or 300 mm-diameter wafers for ULSI substrates requires more detailed information than ever in crystal imperfections, surface strain, or damage in wafers. For this purpose, development of a large-area X-ray topography technique with high sensitivity to these characteristics is especially desirable.

Recently, we have created an experimental apparatus designed to acquire large-area topographs of silicon crystals at the second experimental hutch of beamline BL20B2 at SPring-8 (Chikaura *et al.*, 2001). This set-up uses the horizontally wide (300 mm) monochromatic X-ray beam realised by the 200 m distance between the hutch and the bending-magnet source point [source size: 0.29 mm (H) × 0.04 mm (V)]. This apparatus, with extremely asymmetric reflections, enabled us to obtain X-ray topographs over the whole surface of a 300 mm-diameter 10 mm-thick silicon crystal with one-shot exposure. In addition, we observed surface damage, *e.g.* saw marks induced by slicing and minute scratch patterns caused by polishing (Kawado *et al.*, 2000, 2001).

In this paper we report the difference in surface-strain distribution caused by various steps of silicon wafer manufacturing processes, *i.e.* slicing, lapping, etching, grinding and polishing, in order to optimize the process conditions.

2. Experimental

Wafers were prepared from p-type (B-doped) or n-type (P-doped) 200 mm-diameter CZ silicon crystals with [100] surface orientation and with a resistivity range of 1–10 Ω cm. The crystals were sliced into wafers with a wire saw. The surfaces of the wafers were lapped with #1000-meshed powder, etched with mixed acid and polished mechanically and chemically by the single-sided polish method. This type of polished wafer was designated as A. Wafers of another type, designated as B, were ground with a #3000 whetstone after the etching, and then polished mechanically and chemically. Test samples were picked up at each step of the wafer manufacturing processes. The sample thicknesses are shown in Table 1.

A schematic diagram of the experimental arrangement is shown in Fig. 1. A 300 mm-wide X-ray beam monochromated by the Si(311) double-crystal monochromator in the optics hutch was irradiated with skew incidence on the sample wafer in the second experimental hutch. The sample was fixed without glue onto a flat plastic plate attached on a horizontal-axis precision goniometer of tangential-bar type, as is shown in Fig. 2. The energy of the X-ray beam was tuned to be 21.45 keV to use the asymmetric 511 reflection with a glancing angle of 0.26°, which was much larger than the critical angle for total reflection, 0.08°.

Before recording topographs, rocking-curve measurements were carried out in a 2 × 4 mm area on the sample with a scintillation counter by rotating ω at fixed $2\theta_B$ (θ_B: Bragg angle). Topographs were recorded with a one-shot exposure at the peak position and both wings of the rocking curve for sliced and lapped wafers. On the other hand, step scanning of ω-rotation (angular step of 5 or 10 arcsec) was used for etched, ground and polished wafers since only narrow stripe images were observed in one-shot topographs for these wafers. The

Table 1
Sample thickness.

The test samples were picked up at each step of the following wafer-manufacturing processes. A: slicing (sample 1) ⇒ lapping (sample 2) ⇒ etching (sample 3) ⇒ polishing (sample 5A); B: slicing ⇒ lapping ⇒ etching ⇒ grinding (sample 4) ⇒ polishing (sample 5B).

Sample number	Thickness (μm)
1	880
2	780
3	740
4	725
5A	730
5B	715

 © 2002 International Union of Crystallography • Printed in Great Britain – all rights reserved

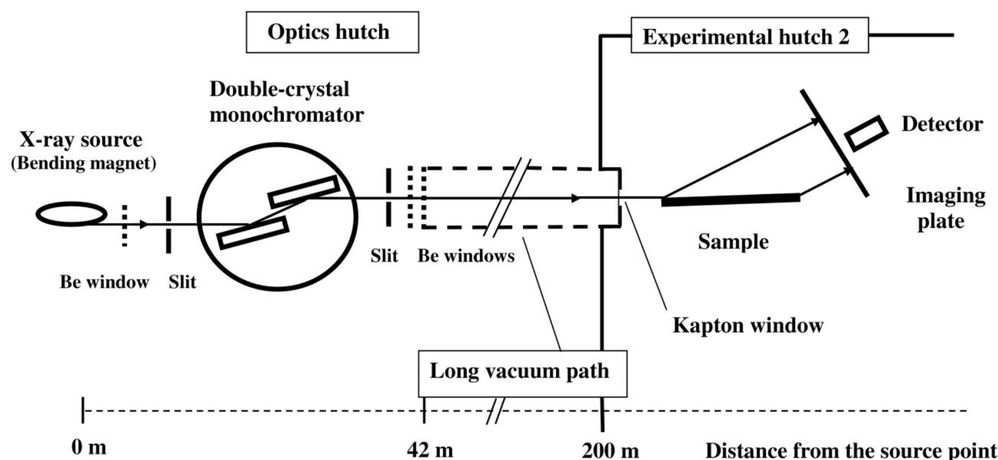

Figure 1
Schematic diagram of the experimental arrangement for large-area X-ray diffraction topography. The 300 mm-wide monochromatic X-ray beam obtained at a point 200 m from the bending-magnet source was used to acquire topographs of a large-diameter silicon wafer sample.

topographs were recorded on an imaging plate with a pixel size of 100 × 100 µm, read by an imaging-plate reader and then processed on a personal computer.

3. Results and discussion

The FWHM (full width at half-maximum) of the rocking curves was useful as a measure of crystallinity although the shape of the rocking curves was influenced by the wavelength spread because of the non-parallel ($+n$, $-m$) setting. Table 2 shows the FWHM of the rocking curves measured at the central position of 200 mm-diameter wafers. The FWHM for etched, ground and polished wafers was about one-tenth as small as that for sliced and lapped wafers. Here it should be noted that the grinding resulted in a rather higher degree of crystallinity.

To evaluate the thickness of the surface layers characterized by the rocking-curve measurements, the depth of X-ray penetration was calculated on the basis of the dynamical theory of X-ray diffraction (Authier, 2001). Since the surface layer of the sliced and lapped wafers was regarded as an imperfect crystal, the X-ray penetration was almost equal to the absorption depth, 5.7 µm. On the other hand, the X-ray penetration into the etched, ground and polished wafers was regarded, on account of their high crystallinity, as the extinction distance for the Bragg case in a perfect crystal, 0.9 µm.

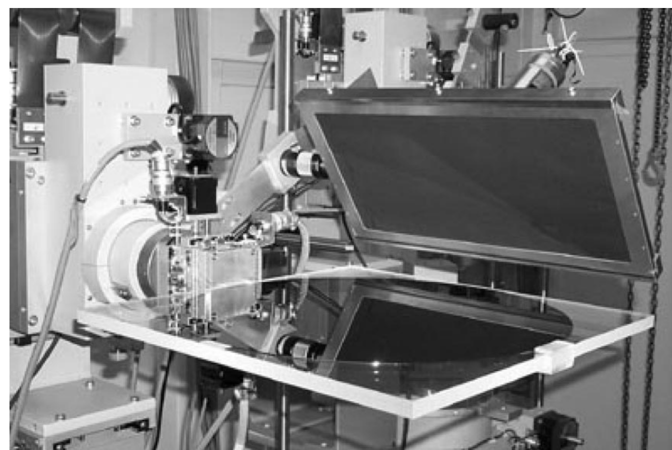

Figure 2
Horizontal-axis precision goniometer equipped with a large sample holder and a large-size imaging-plate cassette.

Table 2
FWHM of the rocking curves measured for silicon wafers with various surfaces.

Sample number	Surface condition	FWHM (arcsec)
1	Sliced	67
2	Lapped	55
3	Etched	4.9
4	Ground	5.1
5A	Polished	3.9
5B	Polished	3.8

Figs. 3(a) and 3(b) show two topographs of the sliced and lapped wafers taken at the peak position of the rocking curve. The whole areas of the wafers were observed with one-shot exposure because of the large FWHM. The warp was found, from the difference in the maximum-intensity positions in the topographs taken at both wings of the rocking curve, to be about 200 arcsec and about 80 arcsec for the sliced and lapped wafers, respectively. This result indicates that the lapping caused a considerable reduction in warp by eliminating residual surface damage such as saw marks.

Figs. 4(a) and 4(b) are step-scanned topographs of the etched and ground wafers, showing so-called zebra patterns (Kikuta *et al.*, 1966). The warp was found to be about 55 arcsec and about 290 arcsec for

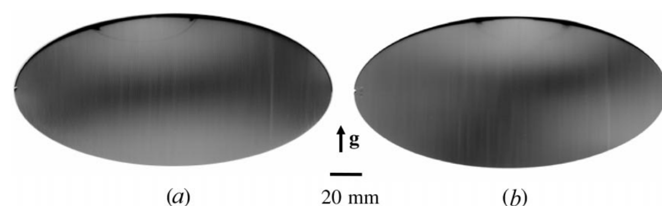

Figure 3
One-shot X-ray topographs: (a) the sliced wafer (sample 1) and (b) the lapped wafer (sample 2). (a) and (b) were recorded using the peak position of the rocking curve measured at the central position of each wafer. The arrow shows the diffraction vector **g** for all the topographs.

the etched and ground wafers, respectively, by counting the number of stripes and the step interval. The etching resulted in a remarkable improvement in local crystallinity and a reduction in warp, while the grinding after the etching caused a marked increment in warp even though good local crystallinity was maintained, as was indicated by the small FWHM.

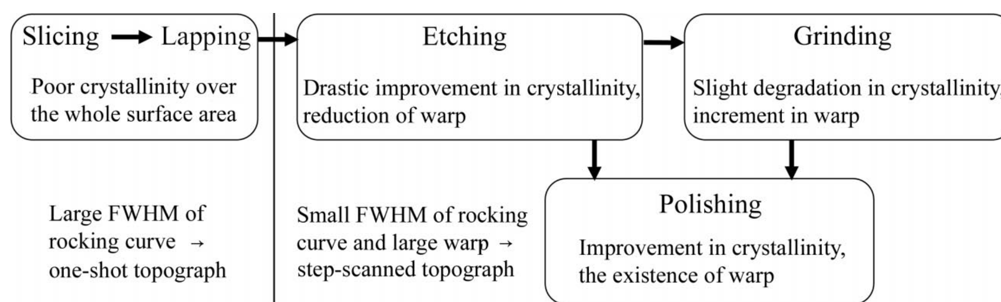

Figure 5
Summary of the X-ray observation and clarified information about surface-strain distribution caused by various steps of the large-diameter silicon wafer manufacturing.

Step-scanned topographs of the two polished wafers designated as A and B are shown in Figs. 4(*c*) and 4(*d*). The warp was found to be about 150 arcsec and about 170 arcsec for A and B, respectively. Much difference in warp was not found between A and B, although the strain distribution in B was influenced by the grinding from the fact that the zebra pattern in Fig. 4(*d*) vaguely resembled that in Fig. 4(*b*). This result means that the grinding is applicable to large-diameter silicon wafer manufacturing processes.

In conclusion, X-ray topography using extremely asymmetric reflection of a 300 mm-wide monochromatic X-ray beam enabled us to obtain some important information about surface-strain distribution caused by the large-diameter silicon wafer manufacturing processes. Clarified effects of the process steps are summarized in Fig. 5.

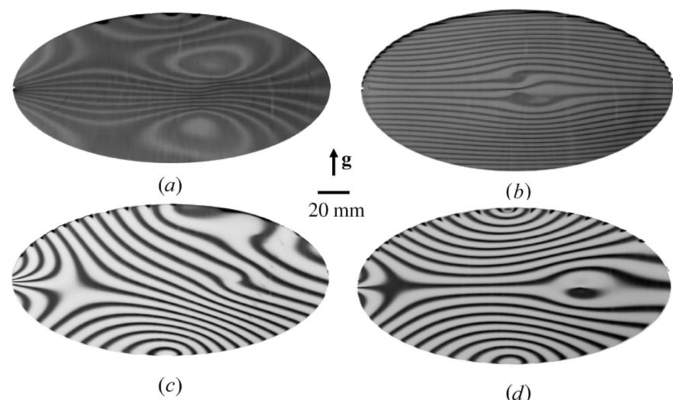

Figure 4
Step-scanned X-ray topographs: (*a*) the etched wafer (sample 3), (*b*) the ground wafer (sample 4), (*c*) the polished wafer A (sample 5A) and (*d*) the polished wafer B (sample 5B). The step interval was 5 arcsec for (*a*) and 10 arcsec for (*b*), (*c*) and (*d*). The arrow shows the diffraction vector **g** for all the topographs.

The authors are grateful to Komatsu Electronic Metals Co. Ltd for supplying the test samples. This work was carried out according to the SPring-8 proposal number 2001A0053-ND-np. Technical support of Drs Y. Suzuki, K. Umetani and K. Uesugi at SPring-8 is also appreciated.

References

Authier, A. (2001). *Dynamical Theory of X-ray Diffraction*, ch. 17. Oxford: Oxford University Press.

Boller, E., Baruchel, J., Pemot, E., Cloetens, P. & Ludwig, W. (1998). *ESRF Highlights 1997/1998*, pp. 84–85. ESRF, Grenoble, France.

Chikaura, Y., Iida, S., Kawado, S., Mizuno, K., Kimura, S., Matsui, J., Umeno, M., Ozaki, T., Shimura, T., Suzuki, Y., Izumi, K., Kawasaki, K., Kajiwara, K. & Ishikawa, T. (2001). *J. Phys. D*, **34**, A158–162.

Chikawa, J., Asaeda, Y. & Fujimoto, I. (1970). *J. Appl. Phys.* **41**, 1922–1925.

Iida, S., Takeno, H., Yagou, Y., Kasagi, N., Sugita, Y. & Kawata, H. (1990). *Defect Control in Semiconductors*, pp. 1529–1534. Amsterdam: Elsevier.

Ishikawa, T. (1989). *Rev. Sci. Instrum.* **60**, 2490–2493.

Kawado, S., Iida, S. & Chikaura, Y. (2001). *SPring-8 Research Frontiers 1999/2000*, pp. 89–91. SPring-8, Hyogo, Japan.

Kawado, S., Iida, S., Ishikawa, K., Chikaura, Y., Suzuki, Y., Kajiwara, K., Kimura, S., Matsui, J., Umeno, M., Shimura, T., Mizuno, K., Ozaki, T., Izumi, K. & Ishikawa, T. (2000). *5th Biennial Conference on High Resolution X-ray Diffraction and Topography (X-TOP 2000)*. Abstracts, p. 107.

Kawado, S., Kojima, S., Kato, Y., Hayashi, H. & Ishikawa, T. (1990). *Defect Control in Semiconductors*, pp. 175–180. Amsterdam: Elsevier.

Kikuta, S., Kohra, K. & Sugita, Y. (1966). *Jpn. J. Appl. Phys.* **5**, 1047–1055.

Kitano, T., Ishikawa, T., Matsui, J., Akimoto, K., Mizuki, J. & Kawase, Y. (1987). *Jpn. J. Appl. Phys.* **26**, L108–110.

Kudo, Y., Liu, K.-Y., Kojima, S., Kawado, S. & Ishikawa, T. (1997). *J. Electrochem. Soc.* **144**, 4035–4041.

Kudo, Y., Liu, K.-Y., Kawado, S., Zhang, X. & Hirano, K. (2001). *J. Appl. Phys.* **90**, 670–674.

Tanner, B. K. (1976). *X-ray Diffraction Topography*, ch. 4. Oxford: Pergamon Press.

 Received 9 October 2002 • Accepted 20 February 2002